Aalborg Universitet

Modeling and Analysis of 2nd Harmonic Interaction for VSC with Transformer under Saturation Condition

Yang, Dongsheng; Wang, Xiongfei; Blaabjerg, Frede; Sun, Yin ; de Jong, Erik

Modeling and Analysis of 2nd Harmonic Interaction for VSC with Transformer under Saturation Condition

Dongsheng Yang, Xiongfei Wang, Frede Blaabjerg
Energy Technology Department
Aalborg University
Aalborg, Denmark
{ doy,xwa,fbl}@et.aau.dk

Yin Sun, Erik de Jong
Flex Power Grid Lab
Group Technology & Research, DNVGL
Arnhem, the Netherlands
{Yin.Sun, Erik.deJong}@dnvgl.com

Abstract—**This paper investigates the mechanism behind the 2nd harmonic interaction of a transformer connected Voltage-Source Converter (VSC) under saturation conditions. The detail small-signal models of a saturated transformer and a VSC are derived considering their nonlinear behavior. It is revealed that the frequency coupling from the saturated transformer and the PLL in the VSC may form a positive feedback loop and give rise to a 2nd harmonic amplification. The harmonic amplification gain is established herein, which provides an accurate assessment of the 2nd harmonic interaction. This theoretical analysis is verified by a power hardware in the loop laboratory experiment.**

Keywords—harmonic interaction, transformer core saturation, VSC, PLL, frequency coupling.

I. Introduction

The high penetration of power electronics interfaced generators has brought growing dynamic stability issues to the power system that can cover a wide frequency range. Recently, the low-frequency harmonic resonance issues attract much more attention because these resonances can easily propagate through the transmission line over a long distance, and may be strongly coupled with the electrical-magnetic transients of the traditional thermal generation plants. It has been reported that a low-frequency resonance in a wind farm resulted in the shaft torsional vibration protection and thereby the generator tripping in the thermal generation plant 200km away [1]. Therefore, accurate modeling and prediction of such kind of low-frequency resonances are deemed critical to the safe operation of the modern power system.

To address these challenges, the impedance-based approach has been recently developed in [2], which not only provides an intuitive insight of the interactions among the grid-connected converters but also enables to reshape the converter output impedance to stabilize the power system. Different small-signal impedance models are established to characterize the dynamic behavior of the grid-connected converter in different reference frames, including the dq-domain impedance model [3], and the sequence-domain impedance model [4]. It is revealed that the Phase-Locked Loop (PLL) introduces asymmetrical dynamics to the direct and quadrature axes, which results in the frequency coupling effects in sequence-domain, i.e., the one single-frequency perturbation imposed on the grid-connected converter will generate responses at two frequencies that are separated by twice fundamental frequency ($2f_1$) [4]. The frequency coupling effects and the negative resistor behavior of PLL tend to excite low-frequency harmonic resonances under weak grid condition associated with a low Short Circuit Ratio (SCR).

Besides the PLL in the grid-connected converter, the converter transformer can also introduce frequency coupling effects when it is saturated due to grid fault recovery, the sympathetic interaction of the transformers, dc current injection by the converter. Actually already in the 1990s, the so-called "core saturation instability" had been reported in the Line-Commutated Converter (LCC) based High Voltage Direct Current (HVDC) transmission system [5], where the 2nd harmonic generated by the transformer after faults was amplified due to the interaction of the LCC and the saturated transformer. This 2nd harmonic amplification is mainly caused by the dynamic interactions between the ac and dc sides of the LCC-HVDC transmission system and is most likely to occur if the resonance frequencies of the ac and dc side networks are close to $2f_1$ and f_1, respectively [6].

Compared with LCC, the Voltage Source Converter (VSC) topology is more controllable, and suffers much less from the harmonic pollution and reactive power consumption and has found its wide application in large-scale PV farms, offshore wind farm, VSC based HVDC transmission system, the Flexible Alternative Current Transmission System (FACTS), etc. However, to the best knowledge of the authors, the potential hazard of harmonic interaction between the VSC and the nonlinear saturated transformer has not been addressed in the literature yet. This paper aims to fill this gap by investigating the mechanism behind the 2nd harmonic interaction between VSC amd the connected transformer under saturation conditions. The detail models of the saturated transformer and the VSC are derived, and it is revealed that the frequency coupling from the saturated transformer and the PLL in the VSC may form a positive feedback loop that could give rise to the 2nd harmonic amplification.

II. Mechanism of 2nd Harmonic Interaction

Fig. 1 shows a general diagram of a grid-connected, LCL-filtered VSC. The dc-link voltage V_{dc} is assumed to be constant, the converter-side current i_L is fed back for regulation. A PLL is used to synchronize the capacitor voltage to the grid. A transformer T_r is used to step up the voltage at the low-voltage terminals to be connected to the medium-voltage power grid. The turn ratio between the low-voltage-side and high-voltage-side is $N_1:N_2$. The equivalent grid impedance for the transmission line is considered as a simplified series *R-L* model.
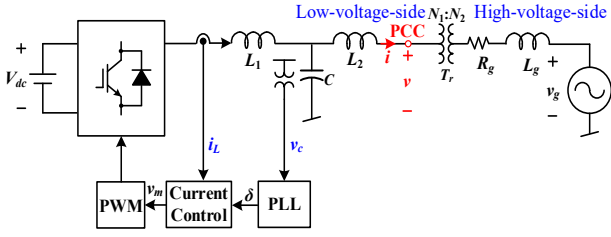
Fig. 1. General diagram of a grid-connected, LCL-filtered VSC with a step-up transformer.
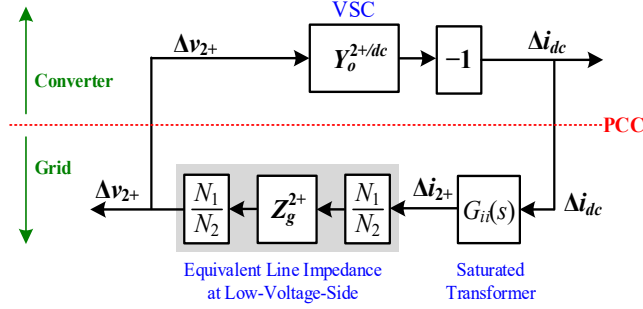

Fig. 2. The basic mechanism of the 2nd harmonic interaction.

When the transformer T_r is saturated, it will give rise to the frequency coupling effects: if an incremental dc current Δi_{dc} is injected into the transformer from the low-voltage-side, this dc current Δi_{dc} will be transferred to the magnetizing current and further increase the saturation level of the transformer. Thus, more harmonic magnetizing currents will be generated which are dominated by 2nd positive sequence harmonic current and the incremental one is noted as Δi_{2+}.

Due to the high impedance at the low-voltage-side that introduced by the current control loop of VSC, Δi_{2+} will only feed into the high-voltage-side and flow through the grid impedance. Therefore, a positive sequence harmonic voltage will be generated at the high-voltage side of the transformer and is then reflected back to low-voltage side, denoted as Δv_{2+}. In summary: an incremental dc current Δi_{dc} injected into the saturated transformer at the Point of Common Coupling (PCC) will generate the incremental positive sequence 2nd harmonic voltage Δv_{2+} at the same point.

As for the admittance model of VSC, the positive sequence/ frequency and negative sequence/frequency components are coupled in the dq domain due to the asymmetrical dynamics of the PLL. In the sequence-domain, however, the frequency coupling occurs at two frequencies that differ by twice fundamental frequency ($2f_1$). It means that, when the positive sequence 2nd harmonic voltage Δv_{2+} is applied on the VSC, a dc current will be generated and flow into the VSC, which has the opposite direction with regards to the dc current injected into the transformer at the PCC point.

According to the abovementioned analysis, a feedback loop is formed due to the frequency coupling effects of the saturated transformers and the VSC, as shown in Fig. 2, where $Y_o^{2+/dc}$ is the coupling admittance of VSC and Z_g^{2+} is the grid impedance at the positive sequence 2nd harmonic frequency, and they are constant complex numbers; $G_{ii}(s)$ represents the transformer saturation dynamics from dc

current Δi_{dc} to the harmonic current Δi_{2+} at the high-voltage-side in an incremental manner. According to Fig. 2, the 2nd harmonic amplification factor can be examined by checking whether the loop gain in (1) satisfies the Nyquist stability criterion.

$$T_h(s) = Y_o^{2+/dc} \cdot G_{ii}(s) \cdot \underbrace{Z_g^{2+} \cdot \left(\frac{N_1}{N_2}\right)^2}_{Z_{g\_eq}^{2+}} \quad (1)$$

It should be mentioned that Fig. 2 only presents the basic mechanism of the 2nd harmonic interaction while some less important dynamics are neglected for easy understanding. In the following sections, the detailed modeling of a saturated transformer and VSC will be established to permit an accurate assessment of the 2nd harmonic interaction.

III. SMALL-SIGNAL MODELING

A. Small-Signal Modeling of VSC

Following the small-signal modeling of the Synchronous Rotating Frame (SRF) based PLL, two dq frames are defined to model the small-signal dynamics of the PLL. One is the grid dq frame that is defined by the phase angle of the fundamental positive-sequence grid voltage $\mathbf{v_g}$, denoted as θ_1. The other is the converter dq frame, which is based on the phase angle obtained from the PLL, denoted as θ. Vectors in the converter dq frame are denoted with the superscript c in the following analysis. As a result, the control block diagram of the L-filtered VSC without considering PLL dynamic can be depicted in Fig. 3(a). where $G_i(s)$ is the current controller, given by:

$$G_i(s) = k_p + k_i \frac{1}{s} \quad (2)$$

$G_d(s)$ represents the time delay of 1.5 times the switching period, which is introduced by the digital computation and PWM implementation, and it can be expressed by:

$$G_d(s) = e^{-1.5sT_s} \quad (3)$$

$Y_L(s)$ is the admittance of the converter-side inductor in the *converter dq-frame*, given by:

$$Y_L(s) = \frac{1}{(s + j\omega_1)L_1} \quad (4)$$

Therefore, the closed-loop response of the control system can thus be given by

$$\mathbf{i_L^c} = \underbrace{\frac{T(s)}{1+T(s)}}_{G_{cl}(s)} \mathbf{i_{ref}^c} - \underbrace{\frac{Y_p(s)}{1+T(s)}}_{Y_{cl}(s)} \mathbf{v_c^c} \quad (5)$$

where $T(s)$ is open loop gain of the current control.

$$T(s) = G_i(s)G_d(s)Y_L(s) \quad (6)$$

Therefore, the control block diagram in Fig. 3(a) can be simplified to Fig. 3(b).
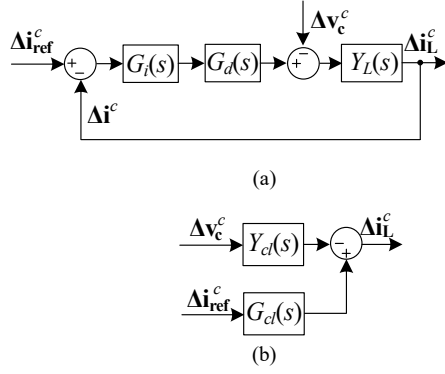
(a)

(b)

Fig. 3. Small-signal model of VSC without considering PLL dynamics (a) Original form (b) Equivalent diagram.
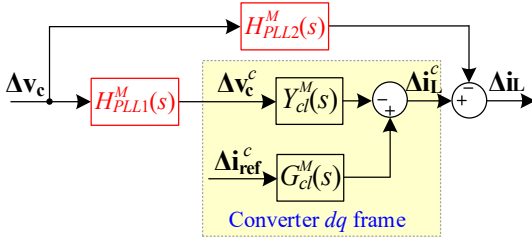

Fig. 4. Small-signal model of VSC considering PLL dynamics

Considering the PLL dynamics, the small-signal model of VSC is shown in Fig. 4, where $H_{PLL1}^M(s)$ and $H_{PLL2}^M(s)$ are the dynamics introduced by the PLL [3], which are given by:

$$H_{PLL1}^M(s) = \begin{bmatrix} 1 & 0 \\ 0 & \dfrac{s}{s + G_{pll}(s)V_{c1}} \end{bmatrix} \quad (7)$$

$$H_{PLL2}^M(s) = \begin{bmatrix} 0 & \dfrac{G_{pll}(s) \cdot I_{Lq1}}{s + G_{pll}(s)V_{c1}} \\ 0 & -\dfrac{G_{pll}(s) \cdot I_{Ld1}}{s + G_{pll}(s)V_{c1}} \end{bmatrix} \quad (8)$$

Moreover, the $Y_{cl}^M(s)$ is the real vector form of $Y_{cl}(s)$, which can be expressed by:

$$Y_{cl}^M(s) = \begin{bmatrix} \mathrm{Re}\left(Y_{cl}(s)\right) & -\mathrm{Im}\left(Y_{cl}(s)\right) \\ \mathrm{Im}\left(Y_{cl}(s)\right) & \mathrm{Re}\left(Y_{cl}(s)\right) \end{bmatrix} \quad (9)$$

where $\mathrm{Re}(Y_{cl}(s))$ and $\mathrm{Im}(Y_{cl}(s))$ denote the real and imaginary parts of $Y_{cl}(s)$.

As a result, the output admittance of the L-filtered VSC in the dq domain is given by:

$$Y_{inv}^M(s) = H_{PLL1}^M(s)Y_{cl}^M(s) + H_{PLL2}^M(s) \quad (10)$$

Therefore, considering the C and L_2, the admittance of VSC seen from the PCC point can be given by:

$$Y_o^M(s) = \left[\left(Y_{inv}^M(s) + Y_C^M(s)\right)^{-1} + Z_{L2}^M(s)\right]^{-1}$$
$$\triangleq \begin{bmatrix} Y_{dd}(s) & Y_{dq}(s) \\ Y_{qd}(s) & Y_{qq}(s) \end{bmatrix} \quad (11)$$

where $Y_C^M(s)$ and $Z_{L2}^M(s)$ are the admittance of C and inductance of L_2 in grid dq frame, respectively, which can be given by:

$$Y_C^M(s) = \begin{bmatrix} sC & -j\omega_1 C \\ j\omega_1 C & sC \end{bmatrix} \quad (12)$$

$$Z_{L2}^M(s) = \begin{bmatrix} sL_2 & -j\omega_1 L_2 \\ j\omega_1 L_2 & sL_2 \end{bmatrix} \quad (13)$$

The dq admittance model of VSC in the real vector form can be equivalently represented by the complex vector form, expressed as:

$$\begin{bmatrix} \Delta i_{dq}(s) \\ \Delta i_{dq}^*(s) \end{bmatrix} = \underbrace{\begin{bmatrix} Y_+(s) & Y_-(s) \\ Y_-^*(s) & Y_+^*(s) \end{bmatrix}}_{Y_{odq}} \begin{bmatrix} \Delta v_{dq}(s) \\ \Delta v_{dq}^*(s) \end{bmatrix} \quad (14)$$

where the asterisk * denotes the conjugation operation, components of the admittance matrix are given by [8]:

$$Y_+(s) = \frac{Y_{dd}(s) + Y_{qq}(s)}{2} + j\frac{Y_{qd}(s) - Y_{dq}(s)}{2}$$
$$Y_-(s) = \frac{Y_{dd}(s) - Y_{qq}(s)}{2} + j\frac{Y_{qd}(s) + Y_{dq}(s)}{2}$$
$$Y_+^*(s) = \frac{Y_{dd}(s) + Y_{qq}(s)}{2} - j\frac{Y_{qd}(s) - Y_{dq}(s)}{2} \quad (15)$$
$$Y_-^*(s) = \frac{Y_{dd}(s) - Y_{qq}(s)}{2} - j\frac{Y_{qd}(s) + Y_{dq}(s)}{2}$$

Therefore, the admittance model of VSC in $\alpha\beta$ frame can be obtained by frequency shifting, expressed by:

$$\begin{bmatrix} \Delta i_{\alpha\beta}(s) \\ \Delta i_{\alpha\beta}^*(s - j2\omega_0) \end{bmatrix}$$
$$= \begin{bmatrix} Y_+(s - j\omega_0) & Y_-(s - j\omega_0) \\ Y_-^*(s - j\omega_0) & Y_+^*(s - j\omega_0) \end{bmatrix} \begin{bmatrix} \Delta v_{\alpha\beta}(s) \\ \Delta v_{\alpha\beta}^*(s - j2\omega_0) \end{bmatrix} \quad (16)$$

By substituting $s=j2\omega_1$ into (9), the relationship between the positive sequence 2nd harmonic and dc component is derived as:

$$\begin{bmatrix} \Delta i_{2+} \\ \Delta i_{dc} \end{bmatrix} = \begin{bmatrix} Y_+(j\omega_0) & Y_-(j\omega_0) \\ Y_-^*(j\omega_0) & Y_+^*(j\omega_0) \end{bmatrix} \cdot \begin{bmatrix} \Delta v_{2+} \\ \Delta v_{dc} \end{bmatrix}$$
$$\triangleq \underbrace{\begin{bmatrix} Y_{11} & Y_{12} \\ Y_{21} & Y_{22} \end{bmatrix}}_{Y_{o\alpha\beta}} \cdot \begin{bmatrix} \Delta v_{2+} \\ \Delta v_{dc} \end{bmatrix} \quad (17)$$

B. Small-Signal Modeling of Saturated Transformer

In order to address the harmonic interaction issue caused by a saturated transformer, the linearized small signal model is established to represent the frequency coupling effects of the transformer caused by the nonlinear core saturation. The equivalent circuit diagram of a single-phase transformer is shown in Fig. 5 as an example, where all the electrical parameters in the high-voltage-side are equivalently transferred to the low voltage side for convenience. R_1 and $L_{\delta 1}$ are the resistor and leakage inductance at the low-voltage-side, respectively; L_m is the averaged magnetizing inductance; and R_2', $L_{\delta 2}'$ are the resistor and leakage inductance at the high-voltage-side. Z_g' and V_g' are the
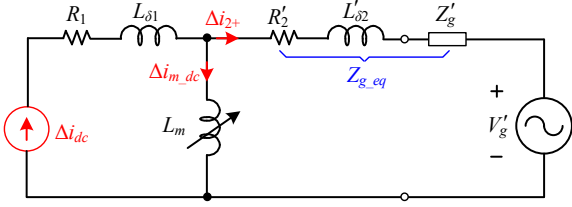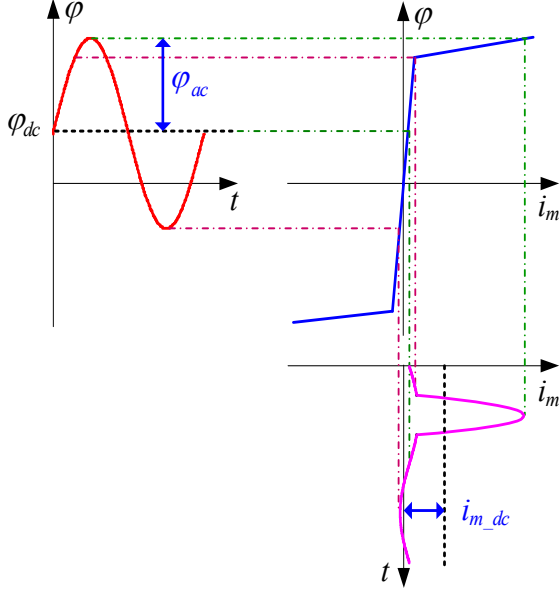
Fig. 5. The equivalent circuit of the transformer

Fig. 6. Magnetizing current under saturation condition

(a)

(b)
Fig. 7. Small-signal model of the whole system

equivalent grid impedance and the grid voltage seen from the low-voltage-side.

When the transformer is not saturated, the magnetizing current flowing through the magnetizing inductor L_m is usually around 1%~2% of the rated current, so typically it can be neglected. However, when the transformer is saturated, as shown in Fig. 6, the magnetizing current will contain a significant amount of 2nd harmonic current including also a dc component.

Moreover, the relationship between the dc component i_{m_dc} and the 2nd harmonic i_{m_2} is linear and is not affected by the magnitude of the ac flux φ_{ac}. It has been proven and experimentally verified that the ratio $k=\Delta i_{m\_2}/\Delta i_{m\_dc}$ remains the same even if the magnitude of the ac voltage applied on the magnetizing inductor is reduced to half of its normal value [7].

The ratio k can be determined through experimental testing. Meanwhile, the dynamic relationship between input Δi_{dc} and Δi_{m_dc} can also be derived according to Fig. 5, expressed as:

$$G_{dc}(s) = \frac{\Delta i_{m\_dc}}{\Delta i_{dc}} = \frac{Z_{g\_eq}(s)}{Z_{g\_eq}(s) + L_m s} \tag{18}$$

$$Z_{g\_eq}(s) \triangleq R_2' + L_{\delta 2}' s + Z_g'(s) \tag{19}$$

Considering the three-phase system, due to the high impedance at the low-voltage-side that introduced by the current control loop of VSC, Δi_{2+} will only feed into the high-voltage-side and flow through the grid impedance.
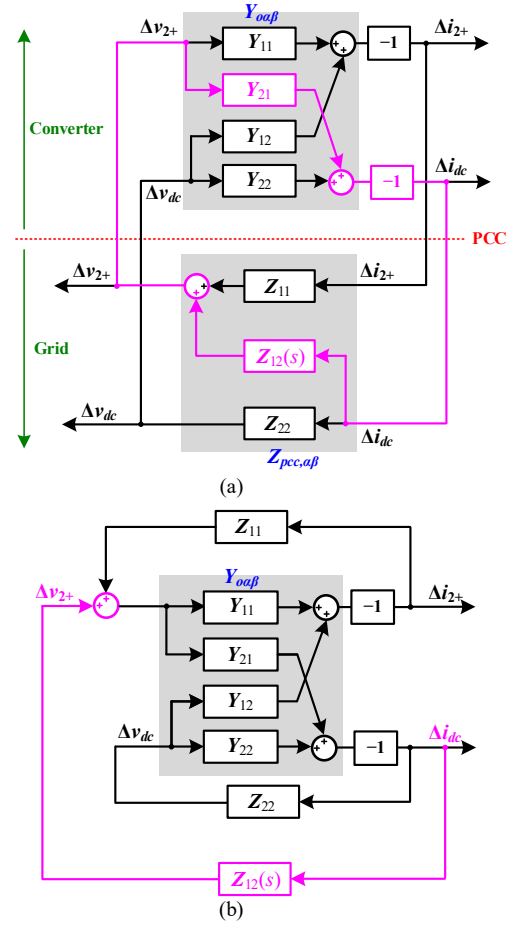
Thus $\Delta i_{2+} \approx -\Delta i_{m2+}$, the dynamic relationship between Δi_{dc} and Δi_{2+} can be derived as:

$$G_{ii}(s) = \frac{\Delta i_{2+}}{\Delta i_{dc}} = -k \cdot \frac{Z_{g\_eq}(s)}{Z_{g\_eq}(s) + L_m s} \tag{20}$$

Therefore, the equivalent grid impedance at PCC can be described by the following transfer function matrix

$$\begin{bmatrix} \Delta v_{2+} \\ \Delta v_{dc} \end{bmatrix} = \underbrace{\begin{bmatrix} Z_{11} & Z_{12}(s) \\ Z_{21} & Z_{22} \end{bmatrix}}_{Z_{pcc,\alpha\beta}(s)} \cdot \begin{bmatrix} \Delta i_{2+} \\ \Delta i_{dc} \end{bmatrix} \tag{21}$$

where ω_1 is the fundamental frequency of the grid, expressed in radians, and the elements of the $Z_{pcc}(s)$ can be expressed by:

$$\begin{aligned} Z_{11} &= R_1 + j2\omega_1 L_{\delta 1} + Z_{g\_eq}(j2\omega_1) \\ Z_{12}(s) &= G_{ii}(s) \cdot Z_{g\_eq}(j2\omega_1) \\ Z_{21} &= 0 \\ Z_{22} &= R_1 \end{aligned} \tag{22}$$

IV.   STABILITY ANALYSIS

According to (17) and (22), the small-signal model of the whole system can be depicted as shown in Fig. 7(a), where the highlighted signal-path is the same as the feedback loop identified in Fig. 2. However, according to the admittance matrices in Fig. 7(a), the system stability can be assessed more accurately. Since all the impedances/

admittances are complex numbers except for $Z_{12}(s)$, Fig. 7(a) can be equivalently transformed into Fig. 7(b). According to Fig. 7(b), the accurate cross-coupling admittance between Δv_{2+} and Δi_{dc} can be derived as:

$$Y_{cs} = \frac{-Y_{21} \cdot (1 + Y_{22} \cdot Z_{22} - Y_{22} \cdot Z_{11})}{(Y_{11} \cdot Z_{11} + 1)(Y_{22} \cdot Z_{22} + 1) - Y_{12} \cdot Y_{21} \cdot Z_{11} \cdot Z_{22}} \quad (23)$$

As a result, the 2nd harmonic amplification gain $T_h(s)$ can be expressed by:

$$T_h(s) = -Z_{12}(s) \cdot Y_{cs} \quad (24)$$

V. EXPERIMENTAL VERIFICATION

In order to verify the effectiveness of the proposed method for the 2nd harmonic interaction assessment, realistic data of the 250kVA, 400V:10kV, Dyn5 distribution power transformer is obtained through a field energization test. After that, the power hardware in the loop system is used to examine the 2nd harmonic interaction when the converter transformer is initially brought to quasi-saturation due to the energization of another transformer nearby, which is usually referred as the sympathetic interaction. The experimental setup contains two parts, as shown in Fig. 8, including the power hardware system and hardware in the loop (HIL) system. The power hardware setup in the DNV GL Flexible Power Grid Lab is made up of a 20 kVA high-bandwidth power amplifier, while the HIL system contains a state-of-the-art real-time digital simulator with high-performance FPGA chip groups.

The parameters of VSC and transformer are shown in Table I and Table II, and the control parameters are shown in Table III. According to parameters, the frequency response of minor loop gain $T_h(s)$ is shown in Fig. 9. As
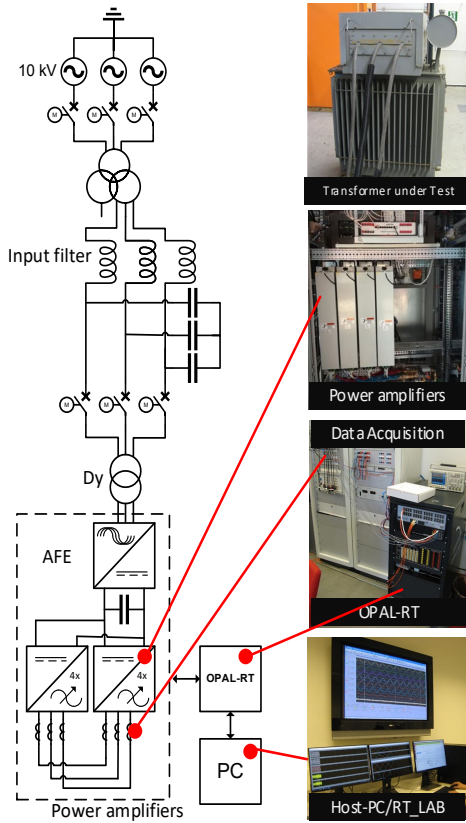
seen, the second order harmonic will not be amplified when the transformer is close to the saturation. The results of the harmonic interaction test are shown in Fig. 10. As seen, due to the dynamic interaction between the saturated transformer and the VSC control system, a low-frequency resonance can be observed in the output currents of the VSC and decays with time. According to the Fourier analysis of the current waveforms, as presented in Fig. 11, large values of the 2nd order harmonic current as well a dc current can be identified, which matches well with that predicted by the theoretical analysis. Therefore, the 2nd harmonic interaction of a transformer connected VSC under saturation conditions is practically verified.
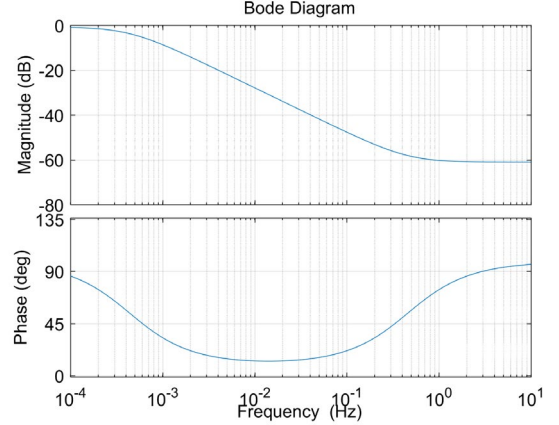

Fig. 9. Frequency response of minor loop gain $T_h(s)$

TABLE I MAIN CIRCUIT PARAMETERS OF VSC

	Parameter	Values
V_{dc}	Input dc-link voltage	800 V
V_1	Rated line to line grid voltage, RMS	400 V
f_1	Grid fundamental frequency	50 Hz
f_{sw}	Inverter switching frequency	2 kHz
f_s	Inverter control sampling frequency	4 kHz
P_n	Rated power	200 kW
L_1	Inverter-side inductor	0.2 mH
C	Filter capacitor	80 μF
L_2	Grid-side inductor	0.03 mH
L_g	Equivalent grid-side inductor L_g (SCR=2)	2.8 mH

TABLE II PARAMETERS OF TRANSFORMER

	Parameter	Values
V_L	Rated voltage at low-voltage side	800 V
V_H	Rate voltage at high-voltage side	400 V
S_n	Apparent Power	250 kVA
f_n	Rated frequency	50 Hz
L_1	Leakage inductance at low-voltage side	40.3 μH
R_1	Winding resistance at low-voltage side	2.8 mΩ
L_2	Leakage inductance at high-voltage side	25.2 mH
R_2	Winding resistance at high-voltage side	1.76 Ω
L_m	Magnetizing inductance at low-voltage side	1.018 H
k	Ratio of $\Delta i_{m\_2}/\Delta i_{m\_dc}$	1.3

Fig. 8. Power hardware loop in the test

	Parameter	Values
k_p	Proportional gain of current controller $G_i(s)$	0.28
k_i	Integral gain of current controller $G_i(s)$	26
k_{p_p}	Proportional gain of PLL controller $G_{pll}(s)$	0.39
k_{i_p}	Integral gain of PLL controller $G_{pll}(s)$	30.8

REFERENCES

[1] W. Wang, C. Zhang, G. He, et al, "Review of measures to mitigate subsynchronous resonance in power systems" *Power System Technology*," vol. 41 no. 4, pp. 1050-1060, April 2017 (in Chinese).

[2] X. Wang, F. Blaabjerg, W. Wu, "Modeling and analysis of harmonic stability in an AC power-electronics-based power system," *IEEE Trans. Power Electron.*, vol. 29, no. 12, pp. 6421-6432, Dec., 2014.

[3] L. Harnefors, M. Bongiorno, and S. Lundberg, "Input-admittance calculation and shaping for controlled voltage-source converters," *IEEE Trans. Ind. Electron.*, vol. 54, no. 6, pp. 3323–3334, Dec., 2007.

[4] M. Cespedes and J. Sun, "Impedance modeling and analysis of grid-connected voltage-source converters," IEEE Trans. Power Electron., vol. 29, no. 3, pp. 1254–1261, Mar. 2014.

[5] S. Chen, A. R. Wood, and J. Arrillaga, "HVDC converter transformer core saturation instability: a frequency domain analysis," *IEE Proc. Gener. Transm. Distrib.*, vol. 143, no. 1, pp. 75-81, 1996.

[6] R. S. Burton, C. F. Fuchshuber, D. A. Woodford, and A. M. Gole, "Prediction of core saturation instability at an HVDC converter," *IEEE Trans. Power Deliv.*, vol. 11, no. 4, pp. 1961–1969, Oct., 1996.

[7] A. Yacamini and J. C. de Oliveira, "Harmonics produced by direct current in convertor transformers," *Proc. Inst. Electr. Eng.*, vol. 125, no. 9, pp. 873-878, 1978.

[8] X. Wang, L. Harnefors, and F. Blaabjerg, "Unified impedance model of grid-connected voltage-source converters," *IEEE* Trans. *Power Electron.*, vol. 33, no. 2, pp. 1775–1787, Feb. 2018.
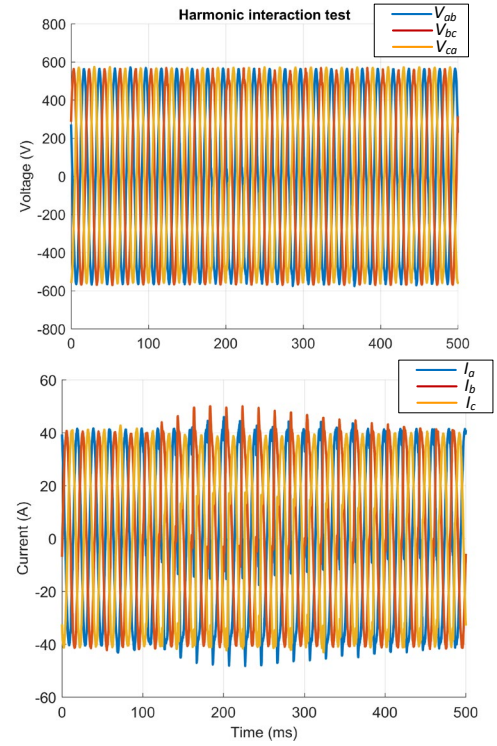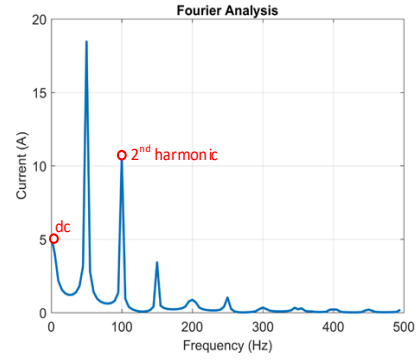
Fig. 10. Waveforms of 2nd harmonic interaction

Fig. 11. Fourier analysis of the injected current waveform